ELSEVIER

Journal of Applied Geophysics 38 (1997) 77–96

JOURNAL OF APPLIED GEOPHYSICS (NLD)

Use of the magnetotelluric method in the study of the deep Maestrichtian aquifer in Senegal

Bernard Giroux [a,*], Michel Chouteau [a,1], Marc Descloîtres [b], Michel Ritz [b]

[a] *École Polytechnique de Montréal, Département de Génie Minéral, C.P. 6079, Montréal, Qué, Canada H3C 3A7*

[b] *ORSTOM-Senegal, Dakar, Senegal*

Received 7 February 1997; accepted 16 June 1997

Abstract

The magnetotelluric (MT) sounding method has been employed to study the deep aquifer of Senegal. Results from nine soundings measured along a 350 km long east–west profile demonstrate that the method provides valuable information about the geometry on the bottom of the Maestrichtian aquifer and that it can be used as a tool for estimating the effective porosity of the aquifer. One-dimensional inversion yields layered models clearly delimiting the bottom of the fresh water aquifer. On the other hand, due to weak electrical resistivity contrasts atop the Maestrichtian sands, the upper limit of the aquifer is not well resolved by MT. However, this limit is generally known from water well data. The effective porosity can be estimated from MT data using Archie's formula if well log data about the pore fluid salt content is provided. Two-dimensional images of the Senegal basin obtained from the nine soundings show geoelectrical features in good agreement with the known geology and hydrogeology. Distortion analysis of the MT impedance tensors and 2D resistivity imaging allow the definition of four main geological features controlling the deep aquifer: the subsidence of the basin, the Linguère fault, the Ndiass horst and the Gassane mafic intrusion. © 1997 Elsevier Science B.V.

Keywords: magnetotelluric; aquifer; Senegal basin; two-dimensional models

1. Introduction

In the last two decades, growing needs for groundwater exploration and characterization has brought new uses to geophysical tools. This is particularly true for techniques that characterize the electrical resistivity of the ground, for it is related to pore fluid salinity and effective porosity (Archie, 1942). This paper describes the application of the magnetotelluric (MT) method to the study of the deep aquifer in Senegal. This aquifer is mainly confined to the Maestrichtian sands (Audibert, 1966), themselves embedded in the thick and conductive sedimentary layers of the Senegalo–Mauritanian basin. The Maestrichtian aquifer is the main source of groundwater in Senegal, being pumped by an increasing number of wells, 328 numbered in 1978 (Forkasiewicz, 1982).

MT was selected over other geophysical methods because it can penetrate conductive sedimentary layers and discriminate salt satu-

* Corresponding author. Tel.: +1-514-340-4991; fax: +1-514-340-3970; e-mail: giroux@geo.polymtl.ca.

[1] E-mail: chouteau@geo.polymtl.ca.

PII S0926-9851(97)00016-5

rated water (very conductive) from fresh water layers. Case histories on the application of the MT, audio- (AMT) and controlled-source audio-magnetotellurics (CSAMT) methods for hydrogeological studies can be found in literature. Chouteau et al. (1994) used MT to study the geometry of the Santa Catarina aquifer in Mexico to find the source of its contamination. AMT is frequently used for groundwater studies. Bernard et al. (1990) used AMT in a volcanic environment on Reunion Island for groundwater investigation; Bartel (1991) used CSAMT in conjunction with hydrology studies to infer a model for fluid flow simulation at the waste isolation pilot plant site near Carlsbad in New Mexico; Nichols et al. (1994) used controlled-source AMT to study a saltwater intrusion in the Salinas valley in California; and, within the framework of hydrogeological studies, Bourgeois et al. (1994) compared AMT with gravimetry and magnetometry for a regional scale structural study of a large sedimentary basin in the Kalahari desert in Botswana. Tinlin et al. (1988) and Brasse (1989) also report the use of AMT for hydrogeological studies.

In this paper, after the geological and hydrogeological characteristics of the Senegalo–Mauritanian basin are introduced, the MT data acquisition and processing procedures are briefly described. Analysis of the impedance tensor and magnetic transfer functions is then carried out to determine the subsurface geometry. Finally, 1D and 2D modelling yield geoelectric cross-sections of Senegal which are discussed in terms of aquifer characteristics.

2. Geological and hydrogeological setting

Senegal is a semi-arid country located in western Africa between longitudes 11°W and 18°W and latitudes 12°N and 15°N (Fig. 1). Most of Senegal is covered by a subsiding sedimentary basin which extends into southern Mauritania. The sediments of Mesozoic age are

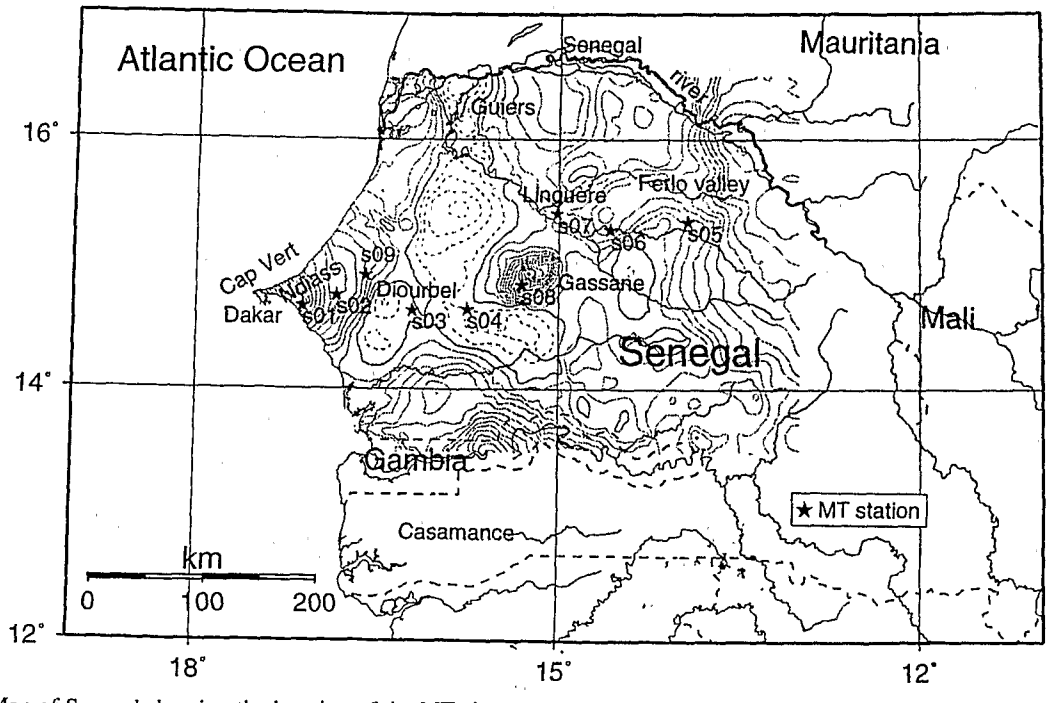

Fig. 1. Map of Senegal showing the location of the MT sites. The Bouguer anomaly (from Liger (1980)) is also plotted for a part of the area investigated. Dashed lines represent negative values of the Bouguer anomaly and solid lines positive values.

thick (~ 8 km) in the western part of the country, especially in the region of Casamance, and thin eastward and northward. Paleozoic rocks outcrop at the south-eastern limit of the country. Most of the Mesozoic sediments (Senonian to Jurassic) consist of sandstones of marine origin which are highly conductive because they are saturated with brines. This sequence is intercalated by layers of clay and limestone of variable thickness (LePriol, 1985; Audibert, 1966). Fig. 2 presents the assumed structure of the basin and of the underlying basement along an east–west profile passing through Cape Verde and extending to Mali. The late Cretaceous sequence (i.e., the Maestrichtian) consists of relatively homogeneous detrital sandy deposits hosting the deep aquifer. The groundwater of this aquifer is weakly mineralized and, consequently, much less conductive than the water below. Overlying this sandy layer is a sandstone of variable thickness which, in turn, is overlain by clay, marl and sand units. The surficial aquifer is embedded in these Tertiary units (Palaeocene and Eocene).

The deep aquifer of Senegal has been called for practical reasons the Maestrichtian aquifer, being found mainly within sands of Maestrichtian age. This is a confined aquifer, except in the Cape Verde peninsula, and the depth to the top of the aquiferous sands is generally more than 100 m, with variations from 0 to 450 m. The Maestrichtian aquifer has an average thickness of 200 m and can provide spot yields of 150 to 200 m^3/h (Forkasiewicz, 1982). Groundwater recharge zones are known to exist along the northern, eastern and south-eastern limits of the basin where the Maestrichtian sands are outcropping and where the Paleozoic bedrock is exposed. Recharge zones are also suspected around the Ndiass horst region and near the intersection of the Senegal river with the Guiers's anticline. Audibert (1971) attributes the natural emptying of the aquifer to vertical flow through the overlying layers which are less permeable but of very large areal extent (200 000 km^2).

Characteristics of the Maestrichtian aquifer are poorly known because most of the information on water quality, hydrogeologic parameters and geometry is provided by a limited number

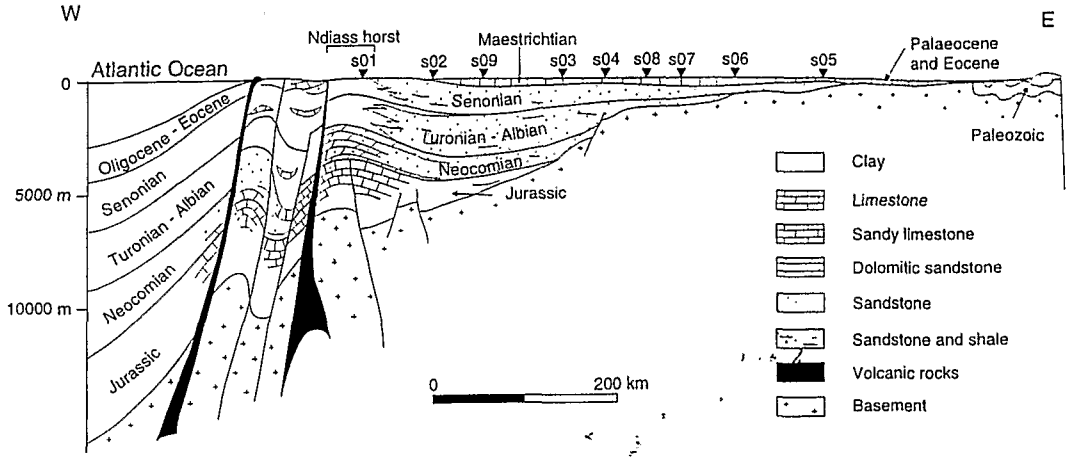

Fig. 2. Schematic geological cross-section along an east–west profile cutting the Senegalese basin from Cape Verde to Mali (from De Spengler et al., 1966). The nine MT station locations are represented approximately as projected along the cross-section profile. The Maestrichtian sands rest on the top of the Senonian formation.

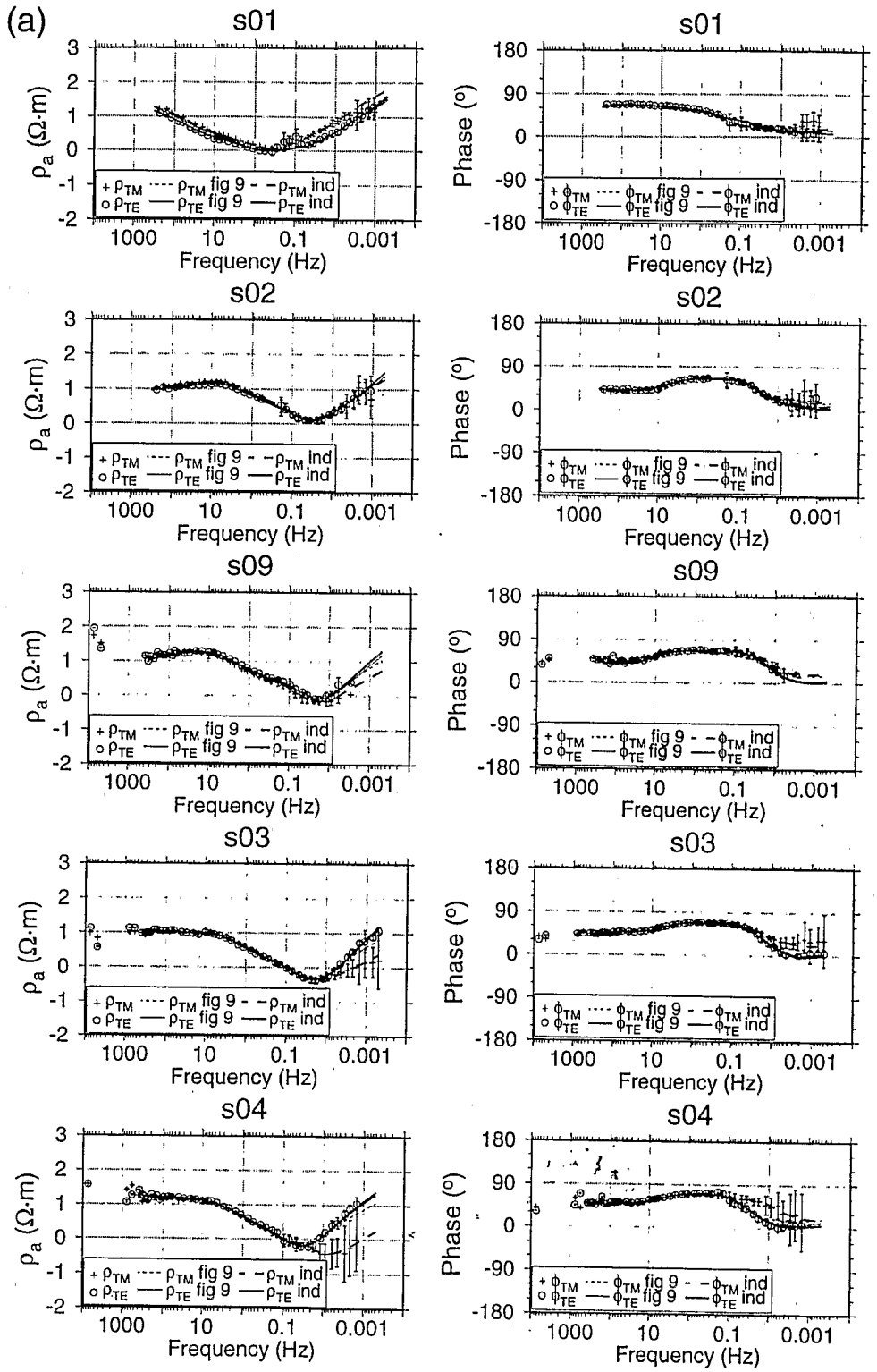
(a)
s01
s02
s09
s03
s04
ρ_a (Ω·m)
Phase (°)
Frequency (Hz)
1000
10
0.1
0.001
+ ρ_{TM} ···· ρ_{TM} fig 9 - - ρ_{TM} ind
○ ρ_{TE} — ρ_{TE} fig 9 — ρ_{TE} ind
+ ϕ_{TM} ···· ϕ_{TM} fig 9 - - ϕ_{TM} ind
○ ϕ_{TE} — ϕ_{TE} fig 9 — ϕ_{TE} ind

Fig. 3.

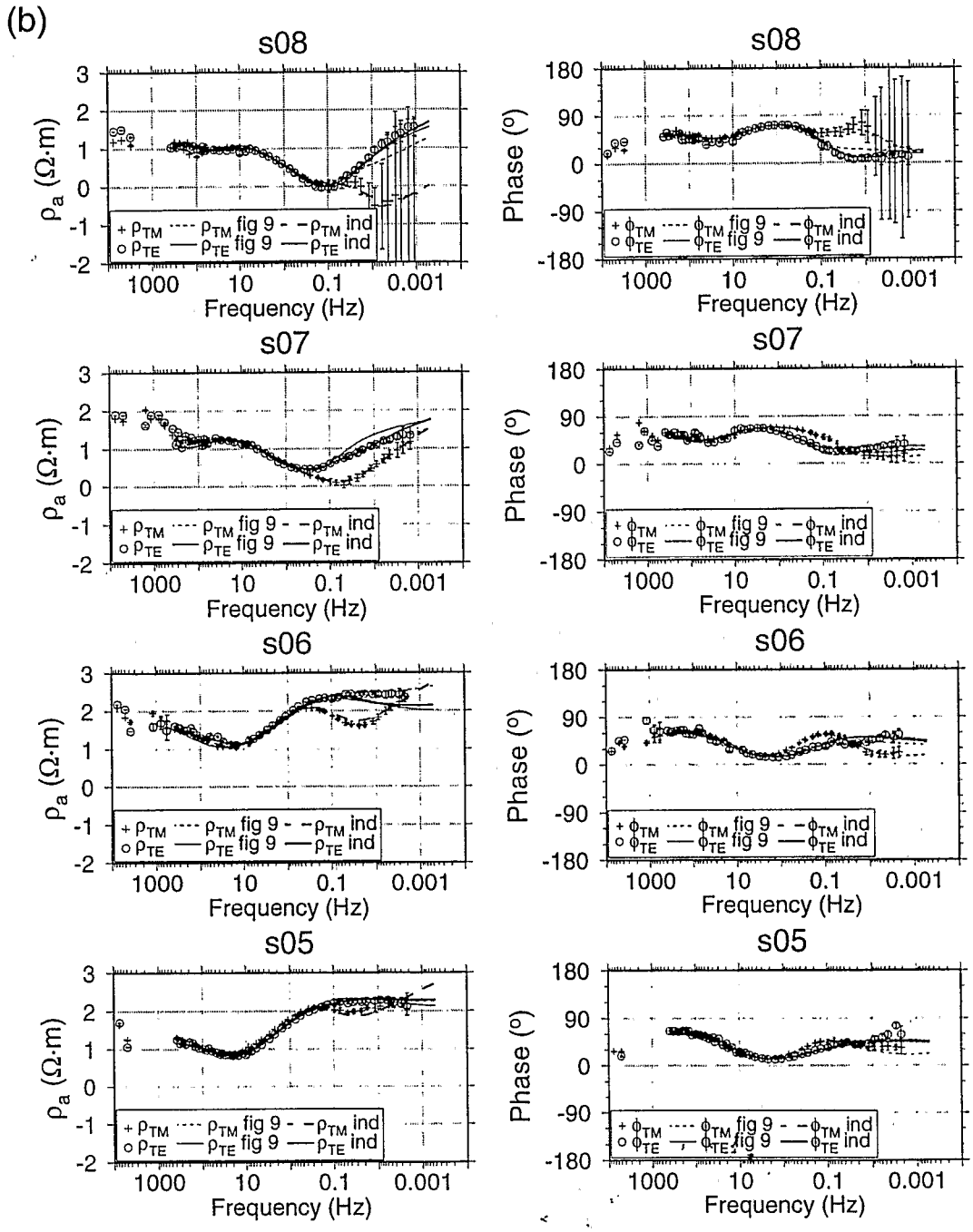

Fig. 3. Apparent resistivity and phase curves for the nine MT soundings from west to east along the profile after rotation to N10°. Phases were all shifted to the same quadrant. This figure also shows the response of the 2D model presented on Fig. 9 (labeled Fig. 9), as well as for both TE and TM independent inversion models shown on Fig. 8 (labeled ind). Error bars are one standard deviation.

of pumping wells coarsely sampling the aquifer over the entire country. Lateral continuity and depth to the bottom of the aquifer remain unknown in most cases. Because the 'effective' bottom of the aquifer is delimited by a fresh water–salt water interface (Audibert, 1966), it is assumed to be easily detectable using DC or EM techniques.

A few geophysical studies have been carried out over the Senegalese basin. Schlumberger DC resistivity soundings were recorded in the 1950's by Compagnie Générale de Géophysique (C.G.G., 1957). They demonstrate the very low resistivity of the top sedimentary layers, which limits the ability of this method to investigate deeply (300–400 m at most with a 6 km dipole). Gravimetric and magnetic data have been interpreted by Liger (1980). His study is concerned with the modelling of the deep basement structures and provides no information about the first kilometer of the basin. However, of particular interest is a very large positive gravimetric anomaly recorded in the Gassane region (near s08 on Fig. 1), extending to Kolobane (s04 on Fig. 1). Resistivity logs were available from oil exploration boreholes drilled in the 1950's and logged with normal (16 in. and 64 in.) and lateral (18 ft 8 in.) resistivity tools. A few of our MT soundings (s02 (borehole Ti1), s03 (DL 1), s04 (KB 1), s07 (Li 1, incomplete) and s08 (Ga 1)) were recorded close enough to these wells to allow comparison between MT models and the resistivity logs.

Long period MT and differential geomagnetic soundings have also been carried out by Ritz (1984), Ritz and Flicoteaux (1985) and Ritz et al. (1989, 1990) in order to determine the deep stratigraphy of the basin together with the crustal structure under Senegal. The interpreted geoelectrical model shows a very conductive monoclinal structure (the Mesozoic sediments) overlying a much more resistive basement (Ritz, 1984). Absence of high frequency data led Ritz et al. to constrain the resistivity of the basin top layer to 15 $\Omega \cdot$ m. No distortion analysis (Bahr, 1991; Groom and Bailey, 1991) was systematically applied to their data, this type of analysis being introduced after publication of their work.

3. Data acquisition and processing

The MT method allows the determination of an electrical conductivity earth model from measurements of natural variations of the surface electric ($\boldsymbol{E}$) and magnetic ($\boldsymbol{H}$) fields over a wide frequency range (see Vozoff, 1972). The method is based on an inductive model of EM energy penetrating into the earth, for which the depth of penetration is both a function of frequency and ground conductivity. The MT complex impedance Z is defined as the ratio $\boldsymbol{E}/\boldsymbol{H}$ and an impedance tensor $\boldsymbol{Z}$ is established from orthogonal and parallel components of $\boldsymbol{E}$ and $\boldsymbol{H}$ such as

$$\boldsymbol{Z} = \begin{bmatrix} Z_{xx} & Z_{xy} \\ Z_{yx} & Z_{yy} \end{bmatrix}, \tag{1}$$

where the first subscript denotes the $\boldsymbol{E}$ component and the second denotes the $\boldsymbol{H}$ component. The magnetic transfer functions relate the vertical magnetic field H_z to its horizontal components (Vozoff, 1972). Sounding curves (see Fig. 3) can be drawn as a function of frequency, in which the complex impedance Z_{ij} is represented as an apparent resistivity and a phase. When the conductivity distribution varies only vertically, the earth model is said to be one-dimensional (1D) and H_z and the diagonal components of $\boldsymbol{Z}$ are null whereas $Z_{xy} = -Z_{yx}$. When in addition the conductivity varies in one lateral direction, the earth is then 2D and the tensor can be rotated such that, for a given 'strike', the off-diagonal components reach a maximum and a minimum value (the diagonal components are still null). The vertical magnetic field is no longer equal to zero. In the 2D case, the TE mode (or E-polarization) has been defined (Swift, 1967) for an $\boldsymbol{E}$ field component in, and an $\boldsymbol{H}$ field component orthogonal to, the

strike direction, whereas the TM mode (or *H*-polarization) has been defined for an $\boldsymbol{E}$ field component orthogonal to, and an $\boldsymbol{H}$ field component in the direction of the strike. When the earth structure is three-dimensional, all the components of $\boldsymbol{Z}$ are usually nonzero. If the scale of the 3D conductive body is small compared to the skin depth (i.e., the depth at which the fields have fallen to $1/e$ of their values at the surface), then channelling of the electric current occurs at a 'local' scale within the conductor and the measured impedance tensor $\boldsymbol{Z}$ is affected by the so-called galvanic distortion (Park, 1985). This effect is frequency independent and will be reflected at all frequencies lower than that at which it first occurs. Bahr (1988) showed that an analysis of the tensor in Eq. (1) can be carried out to recover the inductive information when the local 3D galvanic effect is superposed to a regional 2D model. On the other hand, if the 3D anomaly is localized at the surface, then the entire apparent resistivity curve will be shifted (Jones, 1988) and it is not possible to recover the true resistivity from a single sounding.

Two tensor MT and seven tensor MT-AMT (AudioMT) soundings were recorded along a 350 km east–west profile across the sedimentary basin along the 15° parallel (Fig. 1). The vertical magnetic field was recorded as well. Data were acquired with a V-5 system (Phoenix Geophysics, Toronto) using the remote reference procedure (Gamble et al., 1979). Very good quality data were obtained within the 1000–0.01 Hz frequency band. AMT data (10,000–500 Hz) were of poor quality owing to weak source signals available at the time of the survey. Long period data (0.01–0.001 Hz) show acceptable quality. Good quality data have high field coherencies (> 0.9) and the apparent resistivities and phases show normalized scatter less than 5%. Acceptable quality refers to data with coherencies greater than 0.7 and errors less than 10%. The nine soundings are shown on Fig. 3.

The soundings can be classified into three groups on the basis of similarity of apparent resistivity and phase curves. The first group only includes s01 which was recorded atop the Ndiass horst. Group 2 includes s02, s03, s04, s07, s08 and s09. These sites give measurements typical of the center of the sedimentary basin. The last group consists of s05 and s06 which were recorded in the Ferlo region where the sediments are much thinner.

4. Results and interpretation

4.1. Distortion analysis

A distortion analysis (Bahr, 1991; Groom and Bailey, 1991; Zhang et al., 1993) determined the dimensionality of the conductivity structures, and galvanic effects in the data. The analysis shows that the sedimentary layers can globally be considered 1D and that no galvanic distortion occurs within the frequency range corresponding to the sediments. This range is 1000–0.02 Hz for s02 and is reduced to 1000–10 Hz for s06. Within these frequency ranges for all stations, the Swift (1967) skew κ is lower that 0.1, and the rotationally invariant measure of two-dimensionality Σ (Bahr, 1991) is also smaller than 0.1. The only exception occurs at site s01 (Ndiass horst) where $\Sigma > 0.1$ below 1 Hz, and from 0.1 to 0.001 Hz, the conductivity structure at s01 is weakly 2D, with no galvanic effect and with a weak vertical magnetic field.

Fig. 4 shows the regional skew η (Bahr, 1991) plotted on a pseudo-section as a function of position and frequency. This skew is a phase-sensitive (static shift free), rotationally-invariant measure of dimensionality of the underlying conductivity structure. According to Bahr, values of η higher than 0.3 indicate that the regional conductivity distribution is three-dimensional. A high regional skew is observed in the Senegal dataset around stations s04, s08, s07 and s06 for frequencies lower than 1 Hz (that is, below the sedimentary layers). There is a strong correlation between the high regional skew near s08 and s04 and the gravimetric anomaly of

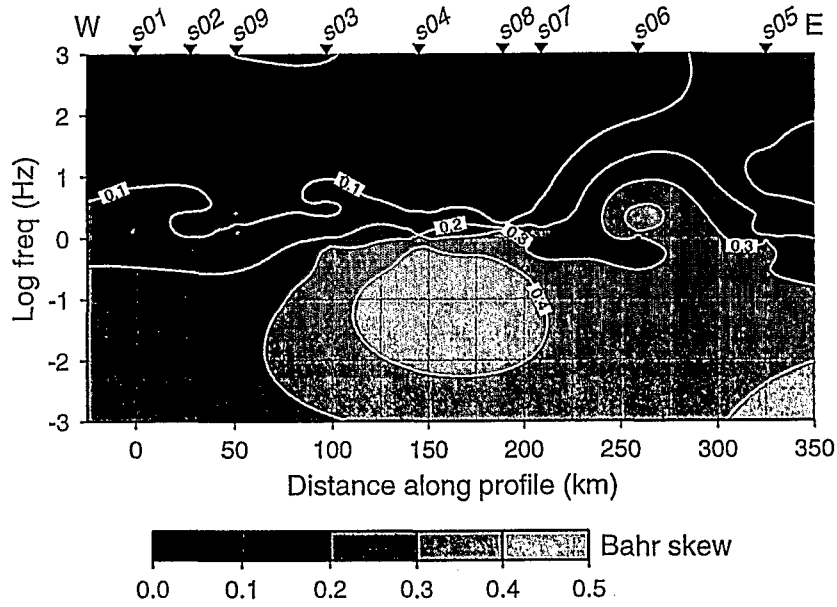

Fig. 4. Bahr 'phase sensitive' skew pseudosection for the nine MT stations projected along an east–west profile. Low values (0.0) of the skew are black, high values (0.4) are light grey.

Gassane which Liger (1980) interprets as a dense mafic intrusion. The high value of regional skew observed around 0.5 Hz under s06 occurs at higher frequencies than that for s08 because the apparent resistivities for s06 are higher and, consequently, the skin depth is larger. The high skew under s06 is suspected to be related to the western termination of a deep horizontal conductor at 20 km depth first observed by Ritz (1984).

Groom–Bailey (GB) impedance tensor decomposition (Groom and Bailey, 1991) can be used to reveal distorsion caused by near surface heterogeneities and to correct MT response. It shows that channelling weakly affects the data. The Groom–Bailey relative error of fit of the tensor decomposition model to the impedance data was calculated over the measured frequency spectrum at all sites for strike angles varying from 0° to 90° in 3° increment as proposed by Groom et al. (1993). Values of GB error were contoured as a function of frequency and rotation angle for each site in order to show if a given strike yields an optimized decomposition. Table 1 shows the strikes obtained employing this analysis and also summarizes Bahr results. It is important to note that for frequencies higher than 1 Hz, the strike is zero or unstable as the resistivity distribution is 1D for all sites. The GB decomposition was applied to data rotated to N10°. The decomposition parameters of twist and shear have low values for

Table 1
Strikes obtained from the distortion analysis

Method	s01	s02	s09	s03	s04	s08	s07	s06	s05
Bahr	$-15° < \theta < 45°$	1D	1D	0°	10°	10°	$-10° < \theta < 45°$	$-45° < \theta < 45°$	$-40° < \theta < -10°$
Groom–Bailey	45°			0°	10°	10°	10°	50°	50°

frequencies corresponding to the sedimentary layers. Also, the twist and shear were small at low frequencies and no sites were found for which these parameters were independent of frequency, indicating that galvanic distortion is weak and that a model consisting of a 3D surficial heterogeneity over a 2D earth model does not apply. The reconstructed GB apparent resistivity and phase were found to be almost identical to the measured data.

Small-scale conductivity heterogeneities can cause amplification or reduction of the telluric field regional response, therefore increasing or decreasing by a constant factor apparent resistivity sounding curves. This effect, named static shift, is negligible for the Senegal data. In fact, superposition of ρ_{xy} and ρ_{yx} for all sites at high frequency show that the resistivity ranges between 10.7 $\Omega \cdot$ m and 16.2 $\Omega \cdot$ m, except at s06 where the apparent resistivity is about twice these values. However, we believe that s06 is free of static shift because ρ_{xy} and ρ_{yx} for this site are superposed, as for all other sites.

The vertical field is null at most frequencies except for stations east of Gassane (s08). Fig. 5 presents two typical magnetic transfer function responses. At s03 the subsurface is 1D and no vertical field is observed in the north–south (A) and east–west (B) transfer functions, where

$$H_z = AH_x + BH_y, \tag{2}$$

and A and B are complex. At s07, a vertical field is observed in the B transfer function. An analysis following Zhang et al. (1993) was carried out in order to evaluate current channelling contributions to the magnetic transfer functions. The analysis showed that at lower frequencies, for sites showing significant vertical magnetic field, vertical field data are a combination of galvanic and inductive responses. The inductive

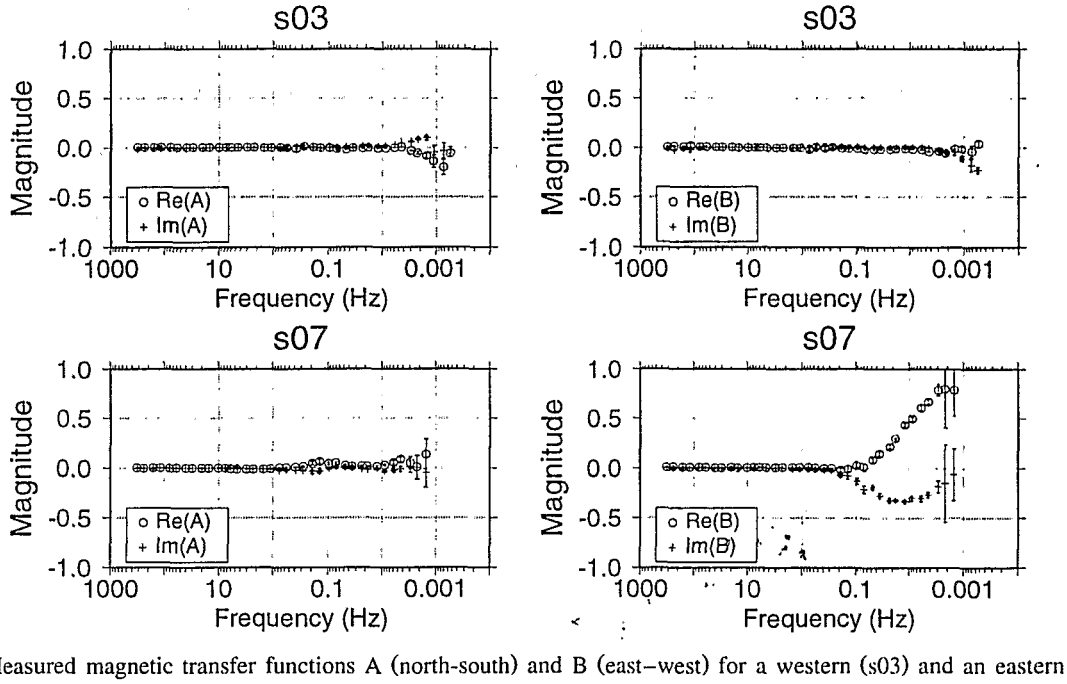

Fig. 5. Measured magnetic transfer functions A (north-south) and B (east–west) for a western (s03) and an eastern (s07) station. The vertical field is very weak at all stations overlying the thick sediments. East of Gassane, a B component is observable at long period.

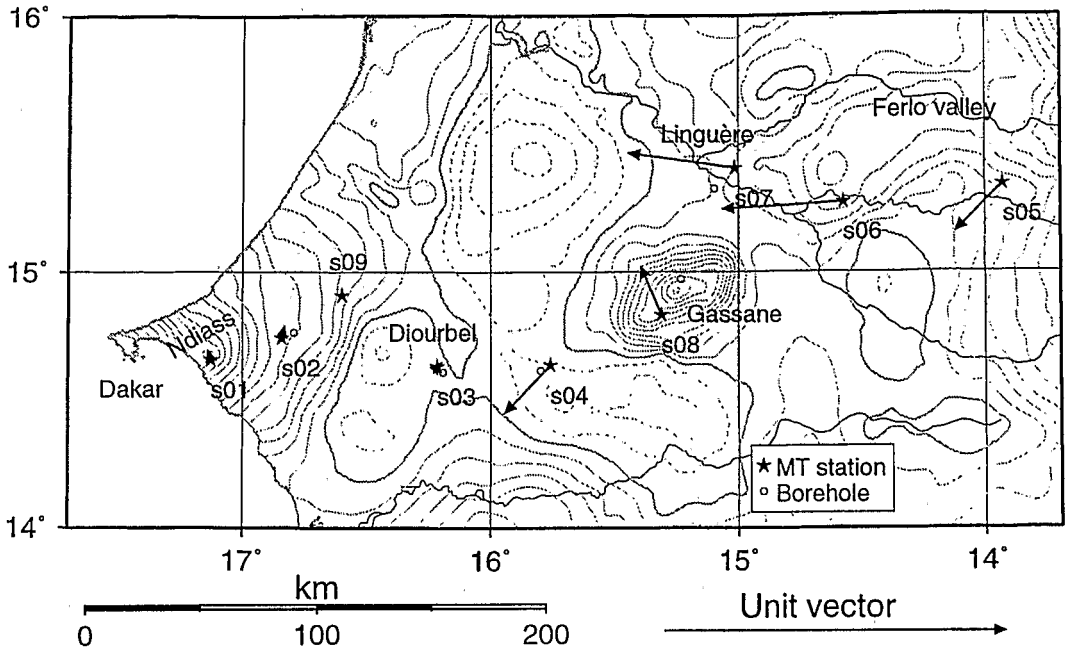

Fig. 6. In-phase induction arrows for 0.0044 Hz A and B data. These arrows were reversed to point toward conductors and corrected for current channeling using the method of Zhang et al. (1993). Note the small magnitude at western stations. The arrows at s07 and s06 point to the west, in the direction of the salt–water wedge. Contours are the Bouguer anomaly displayed in Fig. 1.

component obtained employing this analysis was used to draw induction vectors. When reversed to point toward conductors, the vectors at the eastern stations point at a contact located between meridians 14° and 16° (Fig. 6). These vectors are stronger at Linguère (s07) where a major north–south fault has been mapped (Ritz, 1984), they are pointing toward the basin.

4.2. 1D interpretation

Interpretation in terms of a layered earth can be carried out by assuming a model consisting of a minimum number of layers with sharp conductivity boundaries and by using damped least-squares techniques (Marquardt, 1963) to resolve the layer thicknesses and resistivities from the data. It is the so-called ridge-regression technique (Pedersen and Rasmussen, 1989). The interpretation can also be carried out using a large number of layers, constraining the recovered model to 'minimum structure'. This technique is the so-called Occam 1D inversion implemented by Constable et al. (1987). The former technique is preferred because it yields parameter resolution for the model, and consequently identifies the structures that are supported by the data. Also, observation of resistivity logs often demonstrate that strong resistivity contrasts occur between important lithological units. Discontinuous models from ridge-regression inversion are likely to be more representative of the vertical conductivity distribution within the sedimentary layers than Occam models. Marquardt 1D inversion was carried out on ρ_a and ϕ derived from the determinant impedance Z_{det} (Berdichevsky and Dmitriev, 1976; Park and Livelybrooks, 1989). The initial models for the inversions were visually smoothed versions of the resistivity logs. If no

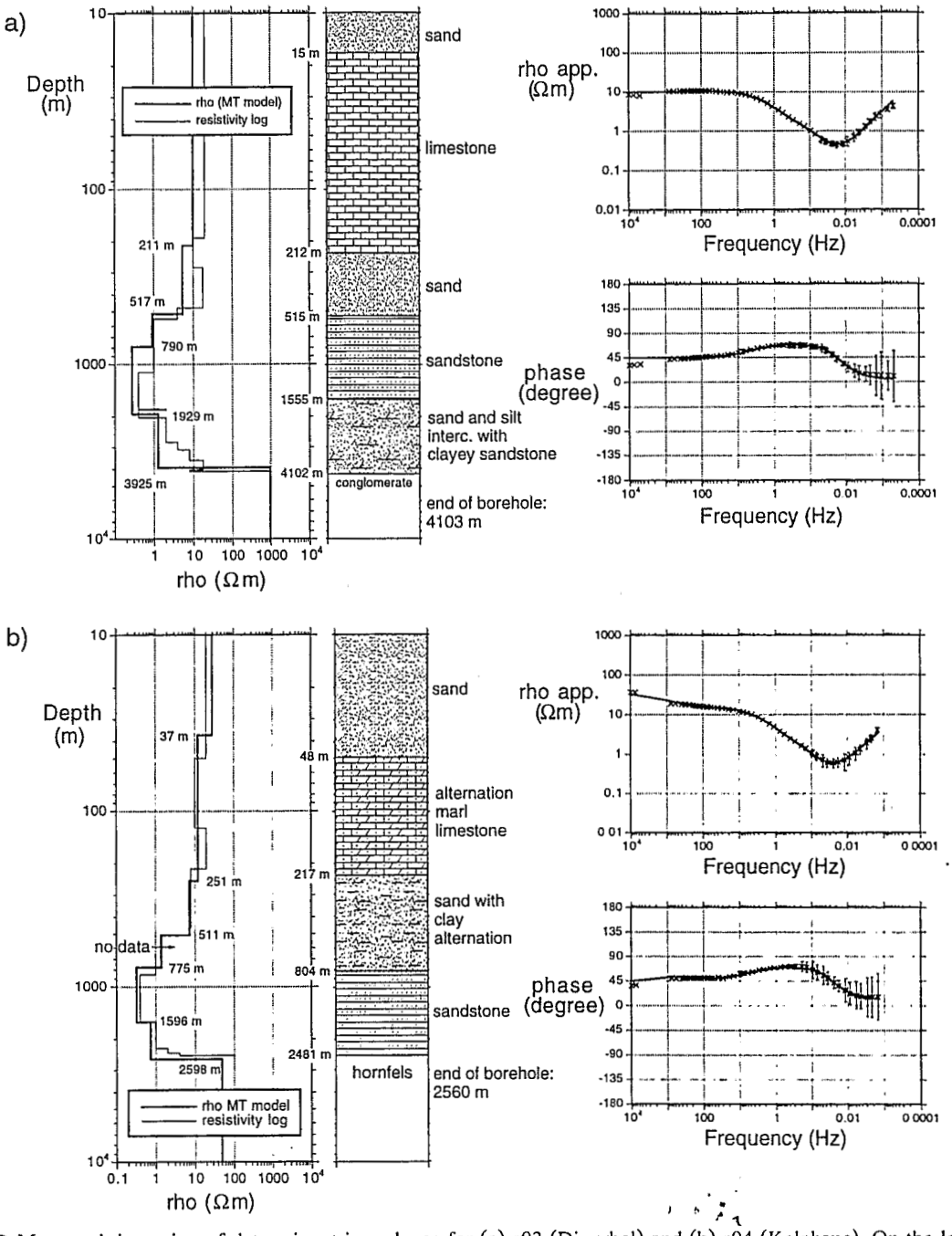

Fig. 7. 1D Marquardt inversion of determinant impedance for (a) s03 (Diourbel) and (b) s04 (Kolobane). On the left is the magnetotelluric model (thick line) and the resistivity log (thin line) recorded in oil wells close to the MT soundings; the depth labels are the depths to the layer boundaries. A schematic representation of the lithology is included for comparison. On the right, the fitting between the measured apparent resistivity and phase (crosses) and the model response (solid line) is displayed.

Table 2
Correlation matrix for s03. Values in italic indicate correlation coefficients of parameters for the same layer

	ρ_1	ρ_2	ρ_3	ρ_4	ρ_5	h_1	h_2	h_3	h_4
ρ_1	1								
ρ_2	0.107	1							
ρ_3	0.054	0.564	1						
ρ_4	0.018	0.176	0.484	1					
ρ_5	0.011	0.103	0.289	0.754	1				
h_1	*−0.176*	−0.894	−0.398	−0.118	−0.069	1			
h_2	0.051	*−0.251*	−0.851	−0.374	−0.222	−0.031	1		
h_3	0.011	0.251	*−0.189*	−0.726	−0.485	−0.226	0.091	1	
h_4	0.019	0.177	0.458	*0.902*	0.957	−0.119	−0.358	−0.614	1

log was available for a given MT sounding, the input model was constructed from known, sometimes incomplete, stratigraphic and lithologic data.

Fig. 7 depicts the 1D inversion models at sites s03 and s04 which have resistivity logs available for comparison. The inversion on s03 was run with the resistivity of the substratum and the thickness of the fifth layer fixed. When these two parameters are left free, tests showed that the inversion underestimated the conglomerate resistivity and, therefore, the depth to the resistive structure was overestimated. For s04, all model parameters were free during the inversion.

1D inversion results show that the fresh water–salt water interface is well resolved by a factor of 10 decrease in resistivity. In fact, correlation matrices (Petrick et al., 1977) for s03 (Table 2 [2]) and for s04 (Table 3) show that the ratio h/ρ for the salt-saturated and underneath layers is well determined since correlation values approach +1. For s03 the interface is at 517 ± 10 m depth, and coincides quite well with the resistivity log (550 m) and the lithological limit between the Maestrichtian sands and Cretaceous sandstone layers. At s04, direct comparison is impossible because no log data is available between 460 and 655 m. Besides, this ability to delimite the fresh water–salt water interface has been demonstrated for all the MT soundings where borehole information was available.

While the lower limit for the fresh water aquifer is easily determined by MT data, the upper limit is poorly resolved. There may be three main reasons for this weak determination: (1) low resistivity contrast between the two media, (2) poor high frequency MT data and (3) reservoir limit not correlated with lithostratigraphic units. The resistivity contrast is very weak if not absent between the Maestrichtian sands and the sediments above (see the resistivity logs in Fig. 7). One could argue, from Fig. 7a and b, that the upper limit could be detected, as resistivity decreases are observed in the models at 211 and 251 m respectively. However, the resistivity ratio for the two layers is less than two and the depth to this boundary drifts considerably during inversion for small changes of the layer resistivities. The shallow layers are less well resolved than the layers overlying the substratum and could be merged into fewer layers, since correlation matrices obtained from Marquardt inversions usually yield values lower than 0.5 for the top two or three layers, as shown in Tables 2 and 3 and in Giroux (1994). One could ask then why models with many layers were used to start inversion. These were dictated by the well log data and the known stratigraphy. Moreover, the poor quality of the AMT data in the frequency range 300–10,000 Hz precludes the resolution of detailed informa-

[2] h_5 and ρ_6 are absent because fixed during inversion.

Table 3
Correlation matrix for s04. Values in italic indicate correlation coefficients of parameters for the same layer

	ρ_1	ρ_2	ρ_3	ρ_4	ρ_5	ρ_6	ρ_7	h_1	h_2	h_3	h_4	h_5	h_6
ρ_1	1												
ρ_2	0.113	1											
ρ_3	0.015	0.425	1										
ρ_4	0.009	0.203	0.634	1									
ρ_5	0.003	0.065	0.216	0.527	1								
ρ_6	0.001	0.028	0.090	0.231	0.613	1							
ρ_7	0.000	0.009	0.028	0.071	0.198	0.438	1						
h_1	*−0.415*	−0.748	−0.312	−0.130	−0.041	−0.017	−0.005	1					
h_2	−0.006	*−0.540*	−0.937	−0.492	−0.163	−0.068	−0.020	0.389	1				
h_3	0.016	0.288	*0.026*	−0.654	−0.349	−0.152	−0.045	−0.242	−0.280	1			
h_4	0.007	0.231	0.648	*0.357*	−0.394	−0.233	−0.069	−0.165	−0.558	−0.109	1		
h_5	0.002	0.043	0.141	0.344	*0.783*	0.964	0.368	−0.027	−0.106	−0.227	−0.290	1	
h_6	0.000	0.007	0.022	0.062	0.246	*0.876*	0.537	−0.004	−0.016	−0.040	−0.089	0.721	

tion about the top layers. As the strength of the signal is unpredictable, it would be wise to use a controlled-source EM technique, such as TDEM, to obtain the needed information. Finally, hydrogeological studies (Audibert, 1966; LePriol, 1985) show that the top of the aquifer sometimes extends into the overlying Paleocene limestone. According to LePriol (1985), tectonic forces acted during the Quaternary to cause collapse or uplift sections of the sediments. The scale of these structures in the shallow layers can affect water flow between sands and limestones. However, this reworking may not lend to detectable conductivity contrasts using the MT method.

In the absence of clay, the ground resistivity ρ_s can be empirically related (Archie, 1942; Meyer De Stadelhoffen, 1991) to the pore fluid resistivity ρ_w and effective porosity ϕ_e by

$$\rho_s = a\rho_w \phi_e^{-m} S_s^{-2} \quad (3)$$

where S_s is the saturation and a and m are empirical factors. Because the water in the shallow layers is of relatively uniform salt content, the resistivity of the ground will then be mostly a function of the effective porosity of the medium.

For s03 and s04, the correspondence between the MT models and the borehole resistivity data is striking. This is not always the case; at Gassane MT overestimates the depth to the substratum as defined from well logs. In this case, the discrepancy between the MT sounding and the resistivity log might be explained by the large distance (17 km) separating the well from the sounding in a region where the Gassane mafic intrusion is likely to affect the substratum topography.

Archie's formula can be used to estimate either the ground porosity or the water salinity since one value must be known to obtain the other. Using the MT model layer resistivities and estimating the pore fluid resistivities from salinity and temperature information, we were able to compute porosity as a function of depth. We used 22 salinity measurements recorded on borehole logs, and a water temperature derived from a geothermal gradient of 3°C/100 m (Pollack et al., 1991) in order to evaluate the pore fluid resistivity according to charts found in Carmichael (1989). The parameter a of Eq. (3) was set to 0.62, and m can be fixed to 1.72 for moderately consolidated sediments and to 1.95 for strongly consolidated sediments (Carmichael, 1989). Results are shown for Diourbel in Table 4. Our values agree well with sonic measurements (Brun, 1983), except for values below 4000 m within bedrock where a and m are inappropriate. These results, even if not related to the Maestrichtian aquifer (depths greater than

Table 4
Porosities obtained from MT data at Diourbel with Archie's formula

Depth (m)	Salinity (g/l)	Ω · m (MT)	Type of formation	Temp (°C)	Ω · m (brine)	ϕ $m = 1.72$	ϕ $m = 1.95$	Brun's values
1150	105	0.28	sandstone	34.5	0.07	0.33	0.38	0.3–0.5 at 700 m depth
1437	109	0.28	sandstone	43.11	0.06	0.30	0.35	0.3–0.5 at 700 m depth
1785	110	0.28	sandstone	53.55	0.05	0.27	0.32	0.3–0.5 at 700 m depth
2242	110	1.27	sandstone	67.26	0.05	0.11	0.14	0.3–0.5 at 700 m depth
2364	135	1.27	sandstone	70.92	0.05	0.11	0.14	0.3–0.5 at 700 m depth
3172	155	1.27	sandstone and clay	95.16	0.03	0.08	0.11	0.1–0.2 at 2500 m depth
3496	70	1.27	micaceous sandstone	104.88	0.04	0.10	0.13	0.1–0.2 at 2500 m depth
3682	11	1.27	micaceous sandstone	110.46	0.17	0.23	0.27	0.1–0.2 at 2500 m depth
4010	50	951	quartzose sandstone	120.3	0.04	0.00	0.00	0.05 at 4000 m depth
4100	140	951	bedrock	123	0.02	0.00	0.00	0.05 at 4000 m depth

1150 m), are presented to show that MT model resistivities together with salinity data can provide good estimates for the ground porosity.

4.3. 2D model

Impedance distortion analysis indicated that, except in a few cases, one-dimensional earth models were sufficient to replicate MT observations above 0.1 Hz. Data below this frequency, however, have characteristics indicating that a multidimensional (2D or 3D) model is more appropriate. Below 0.1 Hz, MT response depends on the more resistive crystalline basement structure underlying the conductive sediments and structural features such as faults and intrusions displaying conductivity changes will affect data at large distances away from the heterogeneities. Therefore 2D inversion was undertaken using the RRI (rapid relaxation inversion) program of Smith and Booker (1991). The method seeks to minimize the objective function $W_i = \beta_i e_i^2 + Q_i$ in which e_i^2 is the squared misfit, β_i is a trade-off parameter between model structure and misfit. Q_i is the 'relaxation' term

$$Q_i = \int_0^{z_{max}} (z + z_0)^3 \times \left[\frac{\partial^2}{\partial z^2} + \alpha \left(\frac{\Delta_i}{z + z_0} \right)^{\eta} \frac{\partial^2}{\partial y^2} \right]^2_{y=y_i} \ln \sigma \, \mathrm{d}z, \quad (4)$$

where Δ_i is the inter-station distance, z is depth and α and η are parameters to be set by the user. z_0 is introduced to keep Q_i from diverging at the surface. The RRI scheme gives fast convergence to a model and yields robust results (i.e., independent of initial model) for our data. The code is efficient because the lateral gradients of the $\boldsymbol{E}$ and $\boldsymbol{H}$ fields are kept constant during the inversion, allowing faster computation of a 'pseudo-1D' inverse at each site. The lateral gradients are updated after each iteration. The 'relaxation' term is used to put constraints on the horizontal and vertical conductivity gradients. With appropriate values of α and η, Q_i effectively smoothes the conductivity distribution and consequently excludes structures which are not supported by the data. Smith and Booker also use error floors to avoid overfitting the data (Smith and Booker, 1991). Errors lower than the stated error floor are set to this value so the minimisation is not dictated by data with unrealistically small errors. Using error floors, it is also possible to weight phase over resistivity, or TE mode over TM mode, by setting large error floors to the parameter we wish to emphasize less. Finally, the program allows one to fix a goal for misfit at each station, providing a way to give more or less importance to a given sounding with regard to the others.

XY and *YX* impedances are measured respectively along N10° and N100°. In order to in-

clude all the stations for inversion, impedance tensors at s05 and s06 were rotated to N10° despite the results of the distortion analysis (which gave a strike of about N50°, cf. Table 1). The TE and TM modes are associated respectively with the *XY* and *YX* resistivities and phases because the main geological structures in Senegal are striking north–south. 2D RRI inversions were carried out on both TE and TM modes individually, and jointly, for a variety of values for inversion parameters α, η, error floors and misfit goals. Geoelectrical models from separate TE- and TM-mode inversions show common features in the sedimentary basin but differ substantially in the basement structure. Fig. 8 presents the models obtained from TE and TM data inversion using $\alpha = 2$, $\eta = 2$ and error floors of 2% for ρ_a and ϕ. The TE data show a moderately conductive vertical dyke-like feature starting at a depth of 2 km underneath s07 that is not found in the TM inversion. However, a conductive zone centered at a depth of 4 km below s08 appears in the TM model but not in the TE. Also under s06 and s05, at a depth of 10 km, a fairly conductive zone is detected in the TM model that has no equivalent in the TE model. The data fit is excellent for both models, as evidenced by Fig. 3. However, joint TE-TM inversion using equal weighting was unable to produce a model yielding a good fit in the regions where TE- and TM-only models showed the discrepancies discussed

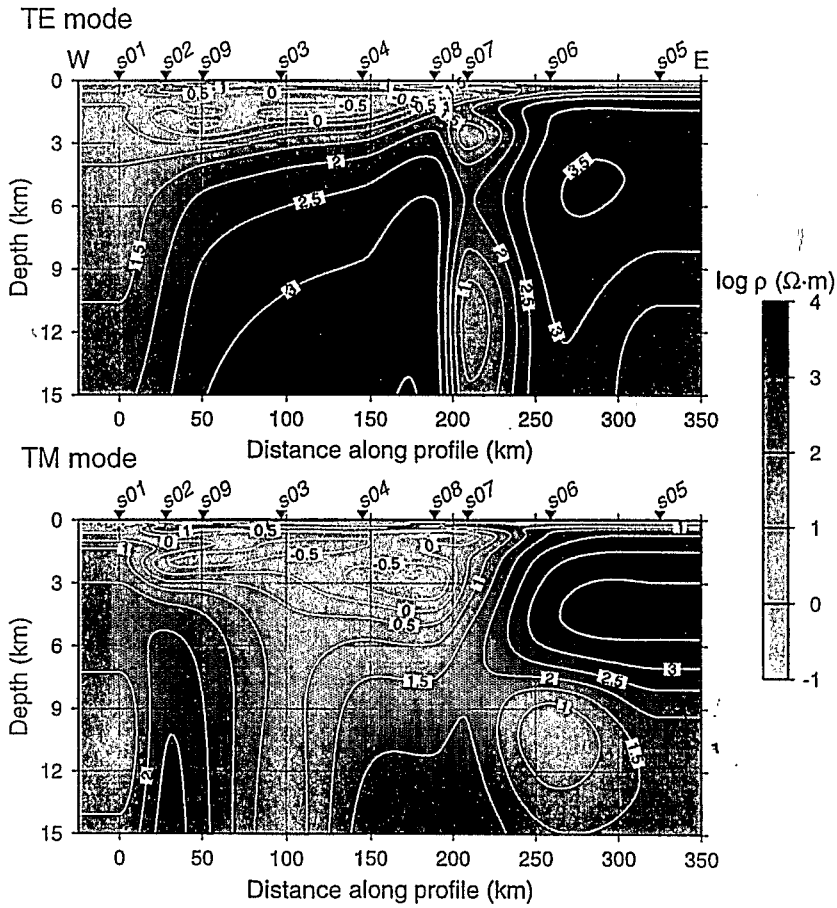

Fig. 8. TE and TM resistivity models obtained for independent RRI inversions on TE and TM data. For both cases, the inversion parameters α and η were set to 2, and the error floors were set to 2%. Contours are in $\log_{10} \rho$.

above. This problem has already been noted by Wu et al. (1993). The TM data (the *yx* data strictly speaking) seems to be the most severely affected by the 3D structure at depth in the vicinity of s08. The reason for this will be discussed later on. Therefore, a joint inversion of the TE-TM data has been carried using low weighting on the TM data. Fig. 9 presents the 2D model obtained using $\alpha = 2$, $\eta = 2$ and error floors of 10% and 2% for ρ_{TE} and ϕ_{TE} respectively and 1000% and 100% for ρ_{TM} and ϕ_{TM}. The main feature is the long conductive body (0.3–3 $\Omega \cdot$ m) lying between 500 and 3000 m depth and located between s02 and s07. This conductor corresponds to the salt-saturated sandstone layer and demonstrates the lateral continuity of this layer. The 2D model shows that an important structure terminates the wedge-shaped conductor under Linguère (s07). This structure is associated with Linguère fault. The basin subsidence to the west is also remarkably depicted by the increasing depth to the bottom of the conductive salt–water structure.

West of the large conductor is a second thinner conductor occurring at a depth between 200 and 600 m (under s01) indicating a major disruption between s01 and the eastern stations. A simple 2D forward modelling showed that the MT data at site s01 are not affected by the conductive Atlantic Ocean located 6 km at least for frequencies higher than 10^{-1} Hz. Therefore, the conductive feature could possibly be associated with a fault bounding the Ndiass horst to the east which, in turn, could be a pathway for recharging the aquifer (Audibert, 1966). Unfortunately, the scale of the survey seriously limits the resolution around this feature and a detailed interpretation is impossible at this stage. A more

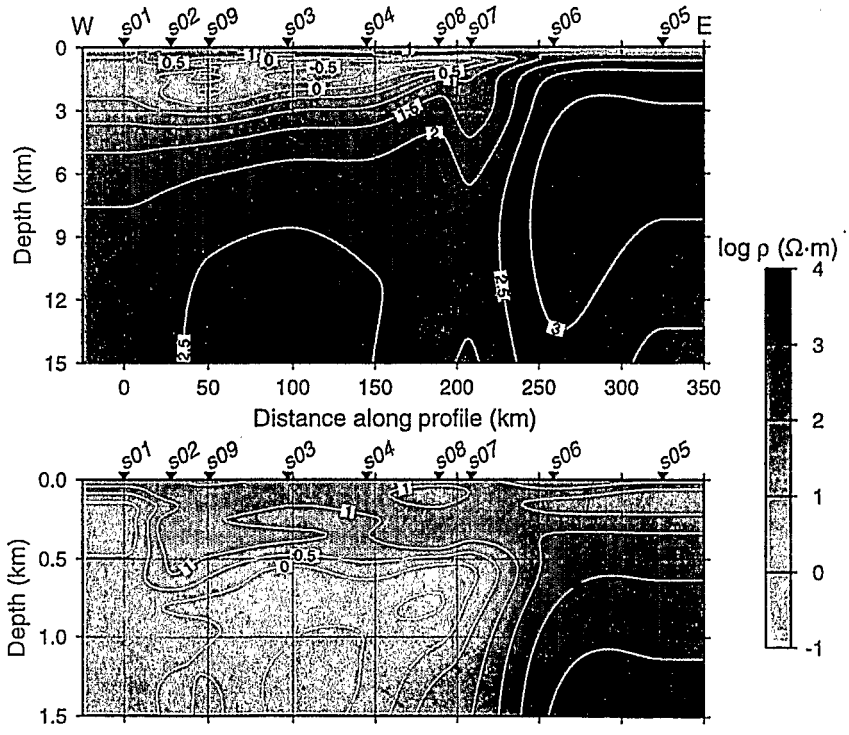

Fig. 9. 2D RRI TE-TM inversion resistivity model of the Senegal dataset. The error floors wee set to 10% for ρ_{TE}, 2% for ϕ_{TE}, 1000% for ρ_{TM} and 100% for ϕ_{TM} during inversion. No static shift correction was applied. Smith and Booker's parameters α and η were both set to 2. The residuals are normalized by the error floor, and therefore they are small because of the large error floors used. The misfit can be better appraised in Fig. 3. The vertical artifact generated under s07 (Fig. 8) has been reduced by setting a higher misfit goal at this station.

detailed MT/TDEM survey has been completed (November 1995) to investigate this zone. Depth to the bedrock evaluated by MT ranges between 2 and 7 km within the basin, depending on the station position with regard to the subsidence. For eastern stations (s05 and s06), the depth to bedrock is believed to lie around 600 m depth.

The basement response requires a more complicated interpretation because of the 3D geometry under s04, s08 and s07 as mapped by high skew values on Fig. 4. The inversion parameters α and η were chosen so as to smooth the lateral variations of ρ in the basement since at 6–15 km depth the resolution is less and the data are noisy. The main feature seen at depth is a vertical, conductive structure under s07 which is more pronounced in Fig. 8 (TE model). It is believed to be an artifact generated by electrical and structural anisotropy in the Mesozoic schists (Giroux, 1994). The artifact in the conductivity model is introduced by the RRI inversion scheme because the modelling routine cannot properly account for the electrical anisotropy. RRI indicates that the strike-oriented component of ρ is conductive relative to the orthogonal direction. On TM models (see Fig. 8), a large circular conductor is always present (whatever the inversion parameters) under s08. In fact, the distortion analysis clearly shows that a 3D body is present under s08, which extends toward s04. This feature in the TM models is generated in the inversion in an attempt to fit a 2D structure response to what is the signature of a 3D resistivity model. Besides, the Gassane intrusion is believed to extend in the east west direction, with a relatively small north–south extension (Liger, 1980), in which case the *XY* data will be related to the TM mode and the *YX* data to the TE mode locally. If the Gassane structure is long enough in the east–west direction to channel currents, 'current starvation' effects (Park, 1985) arise and ρ_{yx} may be suppressed, giving a higher conductivity than is true. Note also that induction arrows for s04 and s08 point somewhat north–south which is consistent with the above model. For this reason and since TM data are less likely affected by 3D structures (Wannamaker et al., 1984), the TE (*XY* or N10°) data was emphasized in the 2D inversion. In order to honour the TM data, another joint TE-TM inversion was carried out using error floors of 10% for ρ_a and 2% (or 0.57) for ϕ for both modes. A misfit goal ranging between 0.1 to 0.3 was attributed to each site except for sites s07 (0.7) and s08 (1.0) which have 3D effects. A good fit is achieved for small values. Fig. 10 shows the resulting resistivity model obtained using α and η set to 2. Most of the features found in the previous model (Fig. 9) are displayed. However, a conductive mass centered

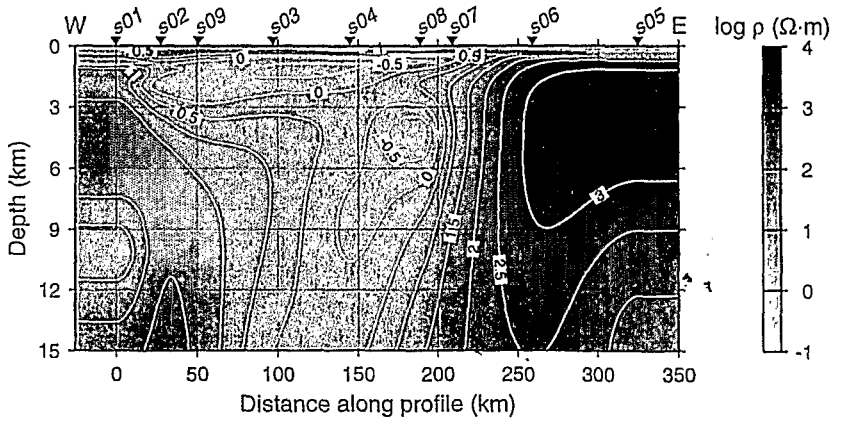

Fig. 10. 2D RRI TE-TM joint inversion resistivity model with error floors of 10% for ρ_a and 2% for ϕ. Other inversion parameters are the same as for the previous inversion (Fig. 9) except for the fit factor that was increased to 1.0 at s08.

below s08 at 4.5 km is still present, a feature found in the TM-only model (Fig. 8) but at 3 km depth.

The Ndiass horst structure is believed to be the cause of the resistivity decrease observed in the basement under s01 at about 10 km depth (Fig. 10). Reworking of the rocks due to thrusting of the horst is likely to have caused an increase of the permeability of the rock, and therefore an increase of the electrical conductivity with the presence of saline water.

5. Discussion

The original motivation for this work was to determine the efficiency of the magnetotelluric method for studying the Maestrichtian deep aquifer. Our results show that, for regional studies, the resolution of the method is sufficient to provide valuable information if the electrical properties of the ground reflect the hydrogeological features. However, the large station spacing along the profile precludes the delimitation of local features as shown, for example, by the data around the Ndiass horst. Nevertheless, 2D models show the major lateral variations of the saline zone beneath the deep aquifer. The modelled geoelectrical sections suggest that the aquifer zone is shallowing in the region of Ndiass and also clearly illustrate the termination of the wedge-shaped salt water layer at Linguère.

When evaluating the effective porosity with Archie's formula, it is important to note that data corrupted by static shift would automatically lead to erroneous estimates of the porosity. For a $\Delta\rho$ shift of the resistivity, the porosity is scaled by

$$\Delta\phi = \frac{-\phi_e}{m\rho_e}\Delta\rho \qquad (5)$$

where m is the cementation factor. Hence, for a static shift of 10% (increase of resistivity), m set to 1.95, ϕ_e is decreased by about 5%, so the static shift effect on the estimation of ϕ_e is less than that for apparent resistivity. One should also note that static shift in MT data biases the determination of depths in resistivity models. This is particularly true for 1D models because the data at one station is not required to be consistent with ρ at adjacent stations as it is in 2D inversion models. This survey again shows the importance of careful analysis of the impedance tensors in order to detect any galvanic distortion and determine the geometry of the subsurface structure.

It is also important to point out that, in this study, the MT method resolves stratigraphic units better than lithological features. Since stratigraphic variations are related to the geological history, they are likely to witness variations of electrical resistivity better than the lithological properties. This is illustrated by the fact that in the Senegalese basin, for instance, the electrical resistivity of the Mesozoic aquifer is mainly function of the water salt content introduced by the marine invasion at that period. On the other hand, lithological properties are dominant in affecting hydrogeological parameters such as hydraulic conductivity, permeability and storage capacity. One has to bear in mind that information provided by MT is of a geoelectrical nature.

6. Conclusions

Results of a nine soundings MT survey over the Senegalese sedimentary basin have shown that the magnetotelluric method can be used as an effective tool to study deep aquifers in electrically conductive subsurfaces as in Senegal. In particular, as confirmed from borehole logs, MT data clearly resolves the bottom limit of the aquifer between the fresh water saturated Maestrichtian sands and the salt water saturated Mesozoic sandstones. The interpretation of the sedimentary layers is fairly straightforward as the conductivity distribution above the basement is generally one-dimensional. MT resistivity

models can also be used, in conjunction with salinity log data, to estimate the effective porosity from Archie's formula.

Two-dimensional interpretation allowed the imaging of the main geological features known to occur within or beneath the Senegal basin: the Ndiass horst, the basin subsidence, the Gassane mafic intrusion and the Linguère fault. These major structures play a significant role in the control of the deep aquifer. The Linguère fault forms an impermeable barrier to the wedge-shaped salt intrusion; the Ndiass horst may be a recharge zone for the deep aquifer; the Gassane intrusion delimits the lower boundary of the aquifer; finally, the subsidence delimits the lower boundary of the deep brine saturated layers.

Acknowledgements

BG wishes to thank Dr. Dean Livelybrooks for helpful comments and discussions on data processing and visualization, and the ORSTOM-Senegal geophysics staff and Magatte Niang for invaluable collaboration during field work. Maps, *xy* plots and two-dimensional sections were plotted using the GMT software (Wessel and Smith, 1991). The authors acknowledge a grant from AUPELF-FICU # 93/PAS/20 which provided the funds to carry out the survey work in Senegal. An NSERC operating grant (OGP0000848) (from M.C.) also provided financial support to BG.

References

Archie, G.E., 1942. The electrical resistivity log as an aid in determining some reservoir characteristics. J. Petrol. Technol. 5.

Audibert, M., 1966. Étude hydrogéologique de la nappe profonde du Sénégal. Tech. Rep. 41, Bureau de Recherche Géologique et Minière, Paris.

Audibert, M., 1971. Fonctionnement hydraulique du système. In: Nappe profonde du Sénégal (Nappe maestrichtienne), BRGM, Paris, pp. 49–65.

Bahr, K., 1988. Interpretation of the magnetotelluric impedance tensor: Regional induction and local telluric distortion. J. Geophys. 62, 119–127.

Bahr, K., 1991. Geological noise in magnetotelluric data: A classification of distortion types. Phys. Earth Planet. Inter. 66, 24–38.

Bartel, L.C., 1991. Results from a controlled-source audiofrequency magnetotelluric survey to characterize an aquifer. In: Ward, S.H. (Ed.), Geotechnical and Environmental Geophysics. Vol. 5 of Investigations in Geophysics, SEG, pp. 219–233.

Berdichevsky, M.N., Dmitriev, V.I., 1976. Basic principles of interpretation of magnetotelluric sounding curves. In: Adam, A. (Ed.), Geoelectric and Geothermal Studies. Akademiai Kiado, Budapest, pp. 163–221.

Bernard, J., Vachette, C., Valle, P., 1990. Deep groundwater survey with audiomagnetotelluric soundings. In: SEG, 60th Annu. Int. Meeting, vol. 60, pp. 528–531.

Bourgeois, B., Mathieu, F., Vachette, C., Vaubourg, P., 1994. AMT measurements compared with gravimetry and magnetometry for structural study of a sedimentary basin: Letlhakeng–Botlhapatlou groundwater project, Botswana. J. Appl. Geophys. 31, 7–25.

Brasse, H., 1989. Audiomagnetotelluric investigations of hydrogeological and tectonic problems in the eastern Sahara. In: M. Gadsden (Ed.), Proc. of the 6th Scientific Assembly of the Int. Assoc. of Geomagnetism and Aeronomy, vol. 53 of IAGA Bulletin, p. 165.

Brun, M.V., 1983. Étude de la subsidence tectonique du bassin sénégalo–mauritanien (Marge ouest africaine). Mémoire de DEA géol. fact sci. tech. St. Jérôme, Université d'Aix-Marseille III.

Carmichael, R.S., 1989. Practical Handbook of Physical Properties of Rocks and Minerals. CRC Press inc., Boca Raton, FL.

C.G.G., 1957. Reconnaissance hydrologique et structurale par sondage électrique au Sénégal, en Mauritanie et en Casamance. Compagnie Générale de Géophysique, Paris.

Chouteau, M., Krivochieva, S., Rodriguez, R., Gonzalez, T., Jouanne, V., 1994. Study of the Santa Catarina aquifer system (Mexico basin) using magnetotelluric soundings. J. Appl. Geophys. 31, 85–106.

Constable, S.C., Parker, R.L., Constable, C.G., 1987. Occam's inversion: a practical algorithm for generating smooth models from electromagnetic sounding data. Geophysics 52, 289–300.

De Spengler, A.J., Castelain, J., Leroy, M., 1966. Le bassin secondaire-tertiare du Sénégal. In: Reyre, D. (Ed.), Bassins sédimentaires du littoral africain, Littoral Atlantique. Symp. Assoc. Serv. Géol. Africain, New Delhi, pp. 80–94.

Forkasiewicz, J., 1982. Aquifere du Maestrichtien du bassin

sedimentaire senegalomauritanien. Bulletin du BRGM (2), III, Bureau de Recherche Geologique et Miniere.

Gamble, T.D., Goubau, W.M., Clarke, J., 1979. Magnetotellurics with a remote magnetic reference. Geophysics 44, 53–68.

Giroux, B., 1994. Application de la magnétotellurique à l'étude des aquifères profonds du bassin sénégalais. M.Sc. thesis, École Polytechnique de Montréal, Que.

Groom, R.W., Bailey, R.C., 1991. Analytic investigations of the effects of near-surface three-dimensional galvanic scatterers on MT tensor decompositions. Geophysics 56, 496518.

Groom, R.W., Kurtz, R.D., Jones, A.G., Boerner, D.E., 1993. A quantitative methodology to extract regional magnetotelluric impedances and determine the dimension of the conductivity structure. Geophys. J. Int. 115, 1095–1118.

Jones, A.G., 1988. Static shift of magnetotelluric data and its removal in a sedimentary basin environment. Geophysics 53, 967–978.

LePriol, J., 1985. Synthèse hydrogéologique du Sénégal 1984–1985. Ministère de l'Hydraulique, Direction des Études Hydrauliques, Division Hydrogéologique, Dakar, 01/85/MH/DEH.

Liger, J.-L., 1980. Structure profonde du bassin côtier Sénégalo–mauritanien. Interprétation de données gravimétriques et magnétiques. Thèse de doctoral, Trav. Lab. Sci. Terre, 16, St. Jérôme, Marseille (B).

Marquardt, D.W., 1963. An algorithm for least squares estimation of nonlinear parameters. J. Soc. Ind. Appl. Math. 11, 431–441.

Meyer De Stadelhoffen, C., 1991. Applications de la géophysique aux recherches d'eau. Lavoisier, Paris.

Nichols, E.A., Morrison, H.F., Lee, S., 1994. Controlled-source magnetotellurics for groundwater. In: SEG, 64th Annu. Int. Meeting, pp. 553–554.

Park, S.K., 1985. Distortion of magnetotelluric sounding curves by three-dimensional structures. Geophysics 50, 785–797.

Park, S.K., Livelybrooks, D.W., 1989. Quantitative interpretation of rotationally invariant parameters in magnetotellurics. Geophysics 54, 1483–1490.

Pedersen, L.B., Rasmussen, T.M., 1989. Inversion of magnetotelluric data: A nonlinear least-squares approach. Geophys. Prosp. 37, 669–695.

Petrick, W.R., Pelton, W.H., Ward, S.H., 1977. Ridge regression inversion applied to crustal resistivity sounding data from South Africa. Geophysics 42, 995–1005.

Pollack, H.N., Hurter, S.J., Johnson, J.R., 1991. A new global heat flow compilation. Dept. Geol. Sci., Univ. of Michigan, Ann Arbor, MI.

Ritz, M., 1984. Electrical resistivity structure of the Senegal Basin as determined from magnetotelluric and differential geomagnetic soundings. Geophys. J. R. Astron. Soc. 79, 635–649.

Ritz, M., Bellion, Y., Robineau, B., 1990. Magnetotellurics applied to the study of the crustal structures in Senegal (West Africa). Geodin. Acta 4, 141–146.

Ritz, M., Flicoteaux, R., 1985. Interprétation d'une prospection tellurique effectuée sur un profil est–ouest à travers le bassin méso-cénozoïque sénégalais. Bull. Soc. Géol. France 8 (I6), 891–897.

Ritz, M., Robineau, B., Vassal, J., Bellion, Y., Dukhan, M., 1989. Structures of the West African craton margin across southern Mauritania inferred from a 450 km geoelectrical profile. Geophys. Res. Lett. 16, 283–286.

Smith, J.T., Booker, J.R., 1991. Rapid inversion of two- and three-dimensional magnetotelluric data. J. Geophys. Res. 96, 3905–3922.

Swift, C.M., 1967. A magnetotelluric investigation of an electrical conductivity anomaly in the southwestern United States. Ph.D. thesis, MIT, Cambridge, MA.

Tinlin, R.M., Hughes, L.J., Anzzolin, A.R., 1988. The use of controlled source audio magnetotellurics (CSAMT) to delineate zones of groundwater contamination: a case history. In: Collins, A.G., Johnson, A.I. (Eds.), Groundwater contamination field methods, vol. 963 of ASTM Spec. Tech. Publ., American Society for Testing and Materials, pp. 101–118.

Vozoff, K., 1972. The magnetotelluric method in the exploration of sedimentary basins. Geophysics 37, 98–141.

Wannamaker, P.E., Hohmann, G.W., Ward, S.H., 1984. Magnetotelluric response of three-dimensional bodies in layered earths. Geophysics 49, 1517–1533.

Wessel, P., Smith, W.H.F., 1991. Free software helps map and display data. EOS Trans. Am. Geophys. U. 72 (441), 445–446.

Wu, N., Booker, J.R., Smith, J., 1993. Rapid two-dimensional inversion of COPROD2 data. J. Geomag. Geoelectr. 45, 1073–1087.

Zhang, P., Pedersen, L.B., Mareschal, M., Chouteau, M., 1993. Channeling contribution to tipper vectors: A magnetic equivalent to electrical distortion. Geophys. J. Int. 113, 693–700.